

See discussions, stats, and author profiles for this publication at: <https://www.researchgate.net/publication/367163020>

Simple Machine Learning with Aerial Imagery Reveals Severe Loss of a Salt Marsh Foundation Species

Preprint · January 2023

DOI: 10.20944/preprints202301.0214.v1

CITATIONS

0

READS

106

4 authors:



Tyler Rippel

United States Environmental Protection Agency

10 PUBLICATIONS 23 CITATIONS

SEE PROFILE



Charles Minsavage-Davis

Georgetown University

8 PUBLICATIONS 7 CITATIONS

SEE PROFILE



Vaughn Shirey

University of Southern California

28 PUBLICATIONS 148 CITATIONS

SEE PROFILE



Gina M Wimp

Georgetown University

76 PUBLICATIONS 3,936 CITATIONS

SEE PROFILE

Article

Simple Machine Learning with Aerial Imagery Reveals Severe Loss of a Salt Marsh Foundation Species

Tyler M. Rippel^{1†}, Charles D. Minsavage-Davis^{1†*}, Vaughn Shirey¹ and Gina M. Wimp¹

¹ Department of Biology, Georgetown University, 37th and O Streets, N.W., Washington, DC 20057, USA; tr599@georgetown.edu (T.M.R.); vms55@georgetown.edu (V.S.); gmw22@georgetown.edu (G.M.W.)

[†]Shared first author

*Corresponding author: cd1231@georgetown.edu; TEL.: +1 (740) 637-1143

Abstract: Salt marshes are globally important ecosystems, but many have been lost or transformed due to the impacts of global change. There have been attempts to broadly quantify salt marsh communities, especially the ubiquitous grasses which serve as foundation species such as *Spartina alterniflora* and *Spartina patens*, the latter of which is being lost due to sea level rise. However, few researchers have used high-resolution geospatial imagery to quantify fine-scale changes in the distribution of grasses or to track losses of *S. patens*. To address this issue, we utilized a simple and rapid method of classifying geospatial marsh imagery with cloud-based machine learning in Google Earth Engine (>92% accuracy for *S. patens* regardless of imagery age). Our methods allowed us to characterize full landscapes (two geospatially proximal areas, >7,000 ha each) of critical salt marshes on the New Jersey coast and to evaluate fine-scale (1-m) community transformations in response to global change with imagery from 2006 to 2019. Notably, one marsh experienced very little change while the other experienced an 81.17% (1,087 ha) loss of *S. patens*, illuminating disparate patterns of change for two geographically proximal ecosystems. Further exploration revealed an association in the loss of *S. patens* with increases in streamflow and total nitrogen content in the rivers that run through each marsh. These results signify the importance of broad-scale ecological studies that evaluate fine-scale community transformations and for management strategies that do not generalize across landscapes of an ecosystem-type.

Keywords: community transformations; species loss; geospatial classification; *Spartina patens*

1. Introduction

Salt marshes are globally important ecosystems for fisheries, carbon sequestration, storm-buffering, and pollutant filtering (Barbier et al. 2011; Chmura et al. 2003; Gedan et al. 2011). These ecosystem services are provided by the grasses that serve as foundation species, or species that fundamentally structure ecosystems (Ellison 2019). However, salt marshes are projected to deteriorate greatly in the face of sea level rise, eutrophication, and coastal development (Deegan et al. 2012; Gedan et al. 2009). There are many modeling (reviewed in FitzGerald and Hughes 2019; Kirwan and Mudd 2012; Simas et al. 2001) and plot-level studies (e.g., Langley and Megonigal 2010; Kirwan et al. 2013; Mueller et al. 2020) demonstrating the potential for multiple global change factors to lead to the dramatic transformation or loss of salt marsh ecosystems. Although some studies have examined the loss of salt marshes at the landscape level (Krause et al. 2019; Wigand et al. 2018) and larger (Campbell and Wang 2020), few studies have detailed ways in which we can repeatedly track vulnerable foundation species in salt marshes, such as *Spartina patens*, over time at the landscape scale.

45% of coastal salt marshes on Earth, if not more, are expected to be lost due to sea level rise, even with drastic reductions in CO₂ emissions (Crosby et al. 2016; Kirwan and Megonigal 2013). Among the areas predicted to suffer substantial losses is the Atlantic coast of the United States, which hosts a substantial proportion of the salt marshes of North America and the world (Mcowen et al. 2017). Previous analysis of mid-Atlantic

coastal salt marshes using remote sensing saw a decline in overall biomass in over 50% throughout the Eastern Seaboard from 1999 to 2018 (Campbell and Wang 2020). Site-level and plot-level analyses have confirmed dramatic losses of salt marshes undergoing multiple global change factors (Alber et al. 2008; Deegan et al. 2012; Schepers et al. 2016; Watson et al. 2017), and have also seen major shifts in foundation species (Zajac et al. 2017). Although some studies have analyzed shifts in foundation species at larger scales (~500 ha; Campbell and Wang 2019), most remote sensing studies in the past have focused on the complete loss of coastal salt marshes or the loss of above-ground biomass, rather than fundamental ecological transformations, such as the loss of *S. patens*.

Along the Mid-Atlantic, *S. alterniflora* and *S. patens* predominate as the foundation species of coastal salt marshes. Notably, both grasses host some common species, such as invertebrates and molluscs, but differ in the unique microbial and animal species that depend on them for food (Denno 1977; Raghukumar 2017; Wimp and Murphy 2021), reproduction (Bayard and Elphick 2011), and microclimate (Gedan and Bertness 2010; Johnson and Williams 2017). Their general layouts on a landscape are regulated by tides: *S. alterniflora* can tolerate daily flooding and therefore has a more extensive range than *S. patens*, which exists at mean-high waterline (Bertness 1991). In some areas, this causes a patchy-mosaic of *S. alterniflora* and *S. patens* with spatial segregation of pure monocultures based on tides (Bertness 1991; Watson et al. 2016), often with large swaths of *S. alterniflora* and interspersed areas of *S. patens* (Figure 1A). *S. patens* has begun declining in respect to *S. alterniflora* (e.g., Zajac et al. 2017), likely due to a lower tolerance of water inundation and nitrogen pollution (Elsley-Quirk et al. 2019; Gedan and Bertness 2010; Snedden et al. 2015; Watson et al. 2016). Considering the unique ecological roles that both species play, and the biodiversity they harbor, tracking the change of *S. patens* on a landscape-scale will be vital for understanding the impacts of global change on coastal ecosystems.

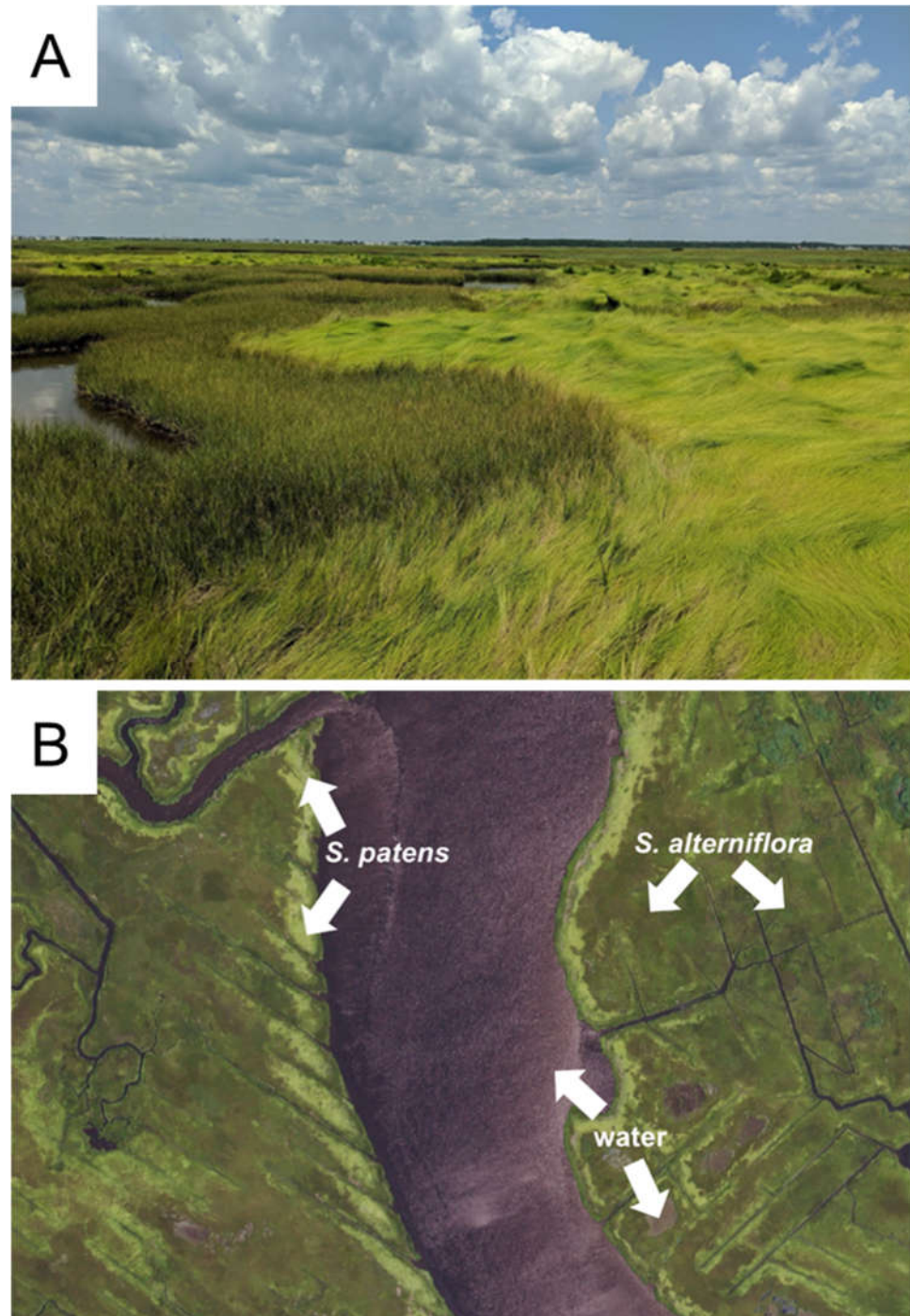


Figure 1. (A) Ground-level photograph at Great Bay Boulevard Wildlife Management Area (39° 33' 16.1'' N, 74° 19' 51.0'' W) depicting the conspicuous juxtaposition of *S. alterniflora* (dark green, upright) and *S. patens* (light green, thatched) found across salt-marshes in coastal New Jersey. Furthermore, note the near monoculture of each grass within their respective patches. Photograph courtesy of Jewel Tomasula. (B) Aerial NAIP imagery (2019) for a *Spartina* spp. dominated marsh, depicting the RGB spectral differences between *S. alterniflora* (dark green, blotched) and *S. patens* (light green, uniform) that aid in ease of identification during geospatial analysis.

Coastal grass species have differences in reflectance qualities across the electromagnetic spectrum, particularly between *S. alterniflora* and *S. patens* (Hardisky et al. 1986), which allows them to be distinguished easily with remote sensing data (Figure 1B). Past studies using aerial or satellite imagery to quantify *S. patens* and *S. alterniflora* have ranged in their success of differentiating the two grasses, using manual digitization, remote sensing, or machine learning (Campbell and Wang 2020; Dahl 2006; Zajac et al. 2017). Artigas

and Yang (2006) used the near-infrared region of the electromagnetic spectrum to successfully differentiate other coastal marsh grasses, but found it most difficult to differentiate between *S. patens* and *S. alterniflora* and did not calculate the areas for any species. With *S. alterniflora* absent, Gilmore et al. (2008) was very successful (92% accuracy) in distinguishing *S. patens* from other coastal marsh grasses using various spectral comparisons (300-2500 nm). Studies involving Unmanned Aircraft Systems (“drones”) and object-based imagery analysis were somewhat less successful in characterizing *S. patens* (72% accuracy; Broussard et al. 2020). Similarly, Artigas and Pechmann (2010) achieved accuracies of 82% for *S. patens* using helium balloons with mounted digital cameras. Other studies did not provide the % accuracy of their classifications or used relatively broad spatial scales (30-m) that do not effectively capture community dynamics in coastal salt marshes (Artigas and Yang 2006; Suir et al. 2020). In general, access to historical “very” high-resolution imagery (VHR at <5-m; Gray et al. 2018) is sparse, given that VHR imagery programs, such as the USDA National Agriculture Imagery Program (NAIP; 1-m resolution), have only been active since 2003 (Adkins 2009). Campbell and Wang (2020) used a limited date range of NAIP (2011-2017) to track changes in salt marsh structure, but did not include the full range available for NAIP or utilize it to identify community transformations.

To date, no study quantifying community transformations between *S. patens* and *S. alterniflora* has been able to utilize VHR imagery over large temporal and spatial scales with publicly available free data sources or with methods which do not require intensive user-side compute resources. Here, we used NAIP imagery (2006-2019) and machine learning techniques on the Google Earth Engine cloud (hereafter GEE) to evaluate community transformations in two expansive coastal salt marshes in New Jersey, with a focus on losses of *S. patens*. New Jersey provides a compelling case study because: (A) sea level rise occurs at 250% the global average (Kopp et al. 2019); (B) the salt marshes of New Jersey are already being transformed (reviewed in Weis et al. 2021); (C) *S. alterniflora* and *S. patens* both occur in vast abundance, with *S. patens* patches existing in a mosaic of *S. alterniflora*; and (D) the dynamics between *S. alterniflora* and *S. patens* have already begun to be altered, favoring *S. alterniflora* (Kennish et al. 2014; Rippel et al. 2020). Our aim was to answer the following questions: (1) Can we consistently and accurately detect transformations in the distribution of foundation species, particularly *S. patens*? (2) Do we find consistent trends between proximal study sites? And (3) can we model these changes using streamflow and nutrient loadings?

2. Methodology

Study Sites

Two study regions were selected after an initial qualitative examination of yearly trends. Our first site (hereafter the northern marsh), Jacques Cousteau National Estuarine Research Reserve and surrounding areas along Great Bay in southeastern New Jersey (7562.95 ha; 39° 33' 20" N, 74° 26' 26" W), has been the subject of numerous ecological studies over the last few decades due to infrastructural access (e.g., roads running through the marsh; Kennish et al. 2014). Our second study site (hereafter the southern marsh), located to the south in the Tuckahoe-Corbin City Fish and Wildlife Management Area (7120.88 ha; 39° 18' 22" N, 74° 41' 42" W), has seen relatively little scientific exploration and only has roads around its border. Despite these infrastructural differences, both marshes are similar in size and show evidence of extensive drainage via ditching (e.g., stark horizontal lining visible from aerial imagery). Based on in-situ knowledge of these areas, both marshes are nearly exclusively dominated by *S. alterniflora* and *S. patens* yet appear to be experiencing vastly different community responses to global change. Thus, the comparison of these marsh communities over time provides us with an opportunity to evaluate response to change in similar ecosystems that are regionally comparable, yet geospatially distinct.

Machine Learning Approach

VHR (1-m) aerial imagery was acquired from the USDA NAIP using Google Earth Engine (Gorelick et al. 2017). NAIP imagery consists of RGB color bands as well as color infrared and NDVI bands and is updated on a continuous 2-to-3-year cycle, with acquisition years varying for different regions of the United States (EROS 2018). NAIP imagery, particularly RGB, is appropriate for our study as it is typically taken between May and September, which aligns closely with the primary growing season of our marshes' dominant grass species and ensures that the disparate colorings of *S. alterniflora* and *S. patens* are effectively captured (Figure 1). We selected all imagery available for our study sites in January 2022, ranging from the most recent imagery accessible at the time of analysis from 2019 to the earliest imagery available from 2006. Thus, the most extreme image sets (2006 and 2019) were utilized for our analyses of overall change, and the years in between (2008, 2010, 2013, 2015, and 2017) to capture the more holistic temporal trends.

Prior to analysis, and for simplicity, we defined three dominant cover classes that were consistent across both sites and represented nearly all variation in cover: *S. patens*, *S. alterniflora*, and water. Water consisted of open water, mud flats, ponding, and other non-biotic coverage as these comparisons were not a focus of this study. For each year, we performed an iterative stepwise selection process in GEE for total number of training and testing data to ensure models did not overfit classes (see methods supplement). A simple classification and regression tree classifier (CART; Krzywinski and Altman 2017) was then applied for the training data at each step, resulting in classifications for every cell on the landscape. From this, we evaluated accuracy of all classes individually and then together using our testing datasets to select the best models, and thus the best representation of class cover, for every year.

Landscape Metrics

We used the 'landscapemetrics' package in R (Hesselbarth et al. 2019; R Core Team 2022) to characterize and compare changes to the structure of *S. patens* patches at our target marshes for 2006 and 2019. We evaluated general metrics (percent cover, number of patches, patch density, average patch size, total core area), connectivity metrics (radius of gyration, landscape shape index, interspersion and juxtaposition), and complexity metrics (total edge, edge density, perimeter-to-area ratio). General metrics were meant to summarize the amounts of *S. patens* that occur within our study sites, and are mostly self-explanatory, except for total core area, which summarizes the amount of total interior of patches that are assumed to be unaffected by edges, with edges set at 1-m. Connectivity measurements were used to understand the ecological connectivity at the landscape level. Radius of gyration is a measure of average patch extent, or how far across the landscape a patch extends. Landscape shape index (LSI) is a ratio of the sum of edge lengths to a minimum total length of edge and increases as increases with more irregular patches. Interspersion and juxtaposition (IJI) measures the distribution of patch adjacencies, where 0 indicates complete separation and 100 indicates a patch is surrounded by all other classes of patches. Finally, complexity metrics were used to summarize the heterogeneity of patches in terms of their interiors and edges. Total edge is the amount of edge habitat in the landscape, edge density is the sum of all edges of a class in relation to the landscape area, and the perimeter-to-area ratio (PARA) is the ratio of edges to interiors.

Forecasting and Evaluating Change

To visually evaluate marsh community shifts between 2006 and 2019, we used geospatial cell subtraction where cells that changed from *S. patens* in 2006 to *S. alterniflora* in 2019 were depicted as a visual difference from cells that changed from *S. alterniflora* to *S. patens* or any other combination. To more comprehensively investigate how *S. patens* has changed over time, we produced a time series for both marshes based on our image classifications for all imagery dates. Current and future trends were forecasted until 2024, 5 years past the most recent imagery date, with a HoltWinters linear technique using the

'forecast' package in R (Hyndman and Khandakar 2008) that was selected due to its simplicity and applicability to distinct data with obvious trends (Green and Armstrong 2015).

Since *S. patens* loss is associated with higher water levels and consistently high nitrogen inputs, we acquired streamflow and nutrient (total nitrogen and total phosphorus) data from the New Jersey Department of Environmental Protection for the most proximal stream gauges for each marsh (Table S1; Lester et al. 2020). We ensured that stream inputs used were from the largest water vectors passing through each marsh: Mullica River for the northern and Great Egg Harbor River for the southern. We specified a suite of mixed-effects models to examine which environmental factors predicted the change in *S. patens* area over: (A) all years for which we had imagery data and (B) all years including years without imagery (using interpolated *S. patens* area values as a response variable for years missing image-derived *S. patens* data). The models included: (1) A model with all predictors and marsh-specific intercepts; (2) a model including only streamflow, total nitrogen (hereafter N), the interaction of streamflow and total N, and a marsh-specific intercept; (3) a model including only streamflow, total N, and a marsh-specific intercept; (4) a model including only streamflow and a marsh-specific intercept; and (5) a model including only total N and a marsh-specific intercept. To decide the best candidate model from this series, for raw and interpolated *S. patens* area values, we compared each model using leave-one-out (LOO) cross-validation (Vehtari et al. 2017). After model selection, we analyzed parameter estimates for our best models using Bayesian credible intervals (Hespanhol 2019). All models were run over 50,000 sampling iterations, 25,000 of which were discarded as warm-up, thinning by 25 across four chains for a total of 4,000 samples from the posterior distribution. We used the "brms" package in R to perform this modeling work (Bürkner 2021).

3. Results

Image Classifications

At equilibrium, the 2019 classification produced the highest overall accuracy for any imagery year with 98.75%, while overall accuracy for the 2006 classification was 93.33% (Figure 2). The lowest overall accuracy for any year was recorded at 90.83% for 2008 (Figure S1). A visual example of changes to an image classification with increasing training points can be found in Figure S2. All classifications consistently produced the highest accuracy for *S. patens* versus any other class, reaching upwards of 100% for 2019 while reaching a slightly lower 94.59% for 2006. *S. alterniflora* and water had similar accuracies within individual years, but still rarely fell below 90% after equilibrium was reached for any given year. These results were confirmed via rigorous qualitative observation of the classifications versus original imagery (example in Figure S3) and were consistent for an increasing number of testing data in our stepwise analysis. Figure 3, created using the image classifications for 2006 and 2019, depicts visual evidence for a drastic reduction in *S. patens* with replacement almost exclusively by *S. alterniflora* in the southern marsh. Visual analysis also revealed that much of the *S. patens* cover in the northern marsh remained unchanged, or became more connected, since 2006.

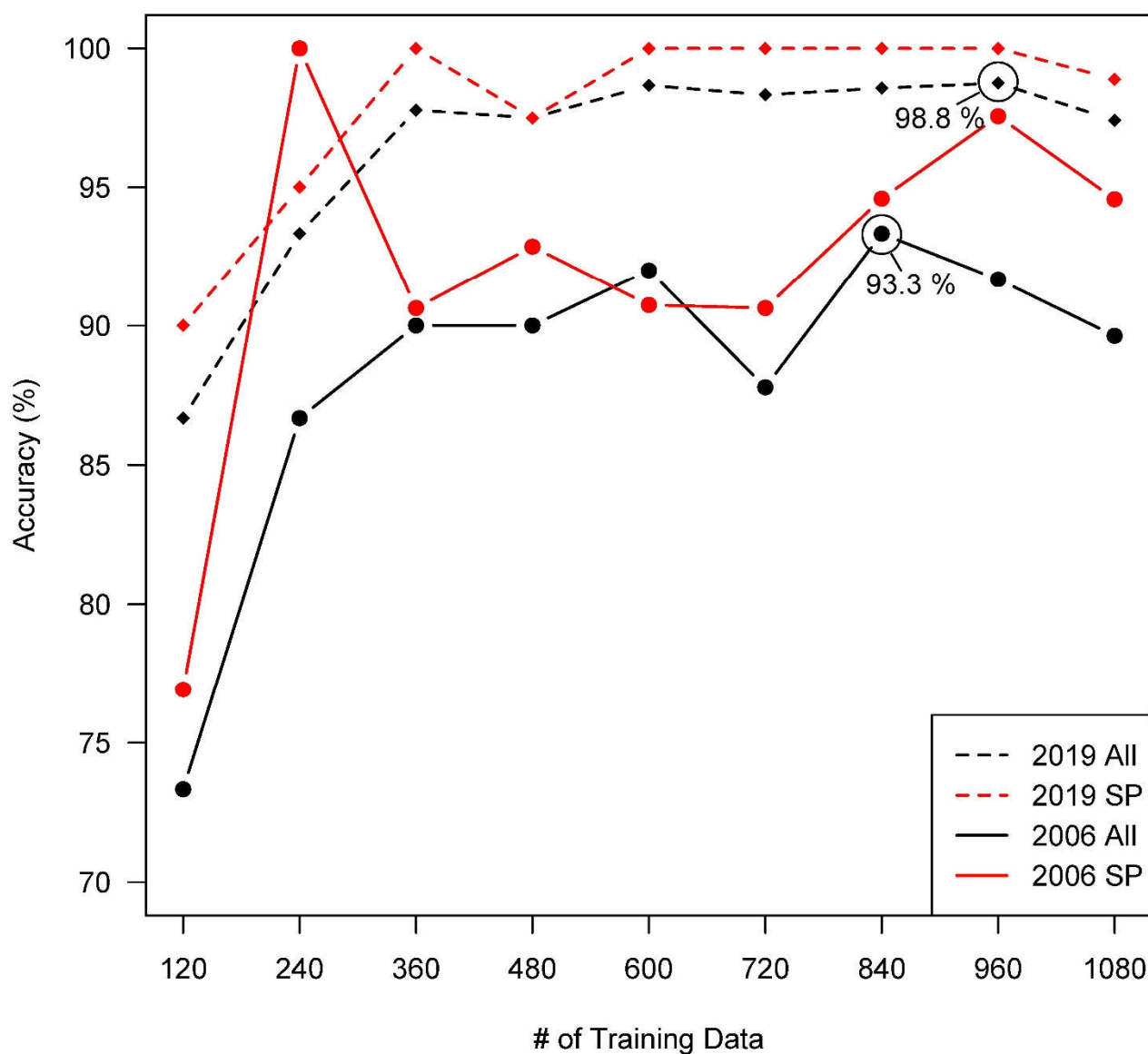


Figure 2. Model accuracy for increasing numbers of randomly partitioned training data used in supervised classification. $X = 1080$ was chosen as a graphical cutoff as it was the entry before over-fitting for the year with the greatest numbers of training data needed to reach equilibrium. 240 for 2006 were a premature peak with low qualitative accuracy when observed. 840 were selected for 2006, even though *S. patens* (SP) was better represented by 960, as it produced the best fit overall model. 100% accuracy for *S. patens* in 2019 is a result confirmed many times over with rigorous visual examination at each reported model step (examples in Figure S2 and S3) as well as with increasing testing data as overall model accuracy increased. I.e., the 960-point training step indeed resulted in 237/240 correct overall tests with 80/80 correct *S. patens* tests. Red lines are only *S. patens*. Created in R, version 4.1.3 (R Core Team 2022).

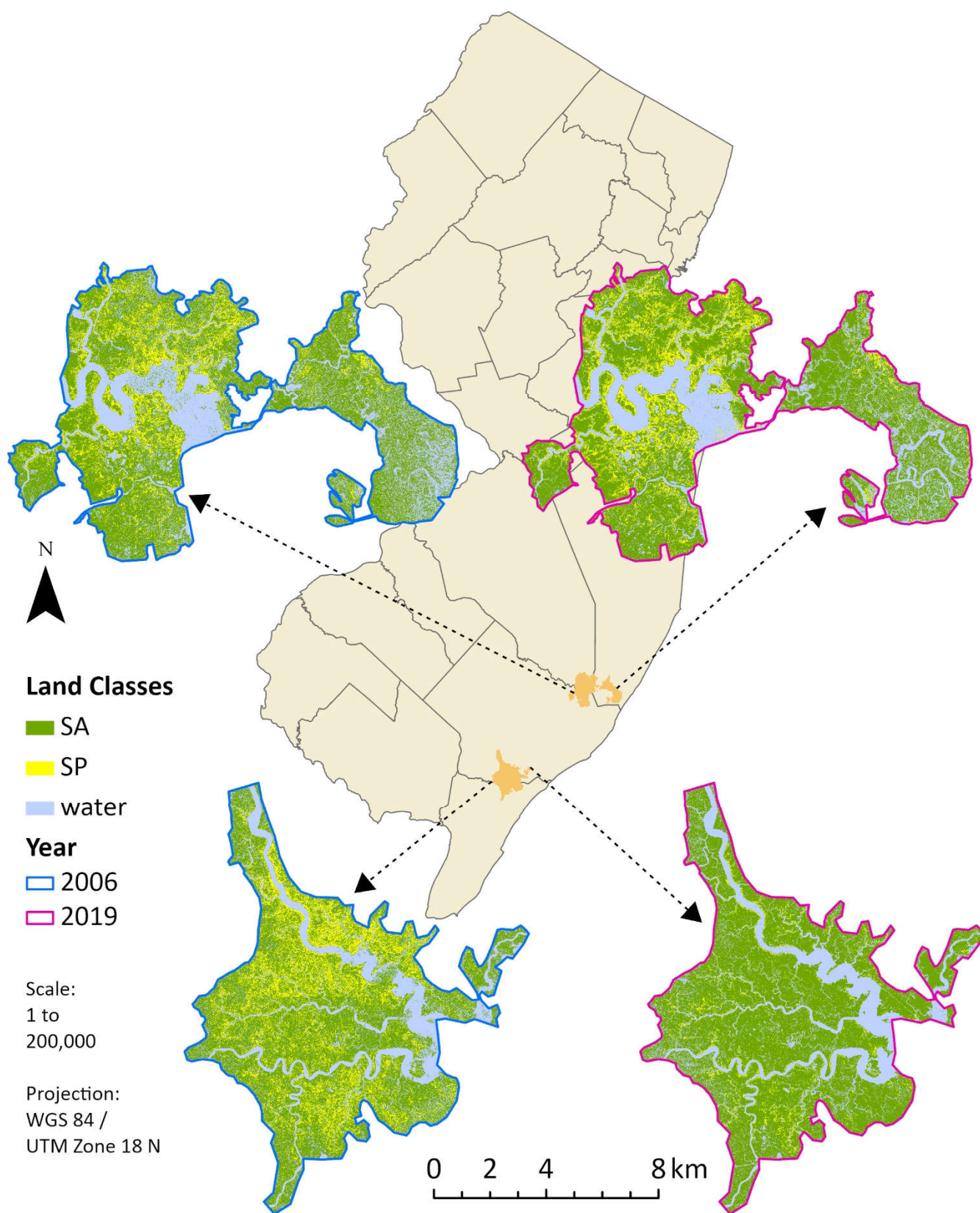


Figure 3. Classified landscapes of our focal marshes and their locations in New Jersey. Northern marsh relative centroid is at $39^{\circ} 33' 20''$ N, $74^{\circ} 26' 26''$ W; southern marsh relative centroid is at $39^{\circ} 18' 22''$ N, $74^{\circ} 41' 42''$ W. New Jersey outline map is not to scale. SA is *S. alterniflora* and SP is *S. patens*. Created in ArcGIS Pro, version 2.9.1 (Esri Inc. 2021).

Landscape Metrics

Our landscape and patch characterizations revealed considerable differences between the northern and southern marshes, as well as between 2006 and 2019 within a marsh (Table 1). Both the northern and southern marshes had decreases in the number of *S. patens* patches (northern: 297361 to 195052, southern: 388377 to 123927) and in patch density (northern: 3934.81 to 2581.01 (100 ha⁻¹), southern: 5454.06 to 1740.28 (100 ha⁻¹)). However, the northern marsh saw increases in percent cover of *S. patens* (11.49% to 12.41%, gain of 7.41%; Figure S4) and radius of gyration (0.89 m to 1.13 m) while the southern marsh had drastic reductions in percent cover (18.80% to 3.54%) from 2006 to 2019 (for a loss of 81.17%) and only moderate gains in radius of gyration (0.91 to 0.94). Thus, it is clear that the northern marsh gained *S. patens* coverage and patches became more connected, which is reflected in the increases in total core area (496.73 to 644.42 ha) and average patch size (29.22 to 48.11 m²), compared to decrease in total core area (770.85 to 133.39 ha) and average patch size (34.47 to 20.34 m²) in the southern marsh. Further, LSI did not reveal drastic differences between the marshes, nor did the complexity measurements (total edge, edge density, perimeter-to-edge ratio). Finally, the southern marsh saw a doubling of its IJI (24.91% to 57.80%), indicating that the southern marsh is now considerably more fragmented with a higher number of small patches surrounded by *S. alterniflora* and/or water, while the northern marsh saw only moderate increases (65.11% to 77.77%) from its much higher initial value.

Table 1. Selected landscape metrics to evaluate *S. patens* over time in our target marshes. LSI is landscape shape index, IJI is interspersed juxtaposition index, and PARA is perimeter-to-area ratio. Cover includes water as a class in the total landscape. Edge depth set to cell size: 1-m for *Spartina* due to small stem radius.

Landscape Metric (Class Level)	Northern Marsh		Southern Marsh	
	2006	2019	2006	2019
Total Area (ha)	868.98	938.56	1338.73	252.08
Cover (%)	11.49	12.41	18.80	3.54
No. Patches (no units)	297361	195052	388377	123923
Patch Density (No. Patches 100 ha ⁻¹)	3934.81	2581.01	5454.06	1740.28
Average Patch Size (m ²)	29.22	48.11	34.47	20.34
Total Core Area (ha)	496.73	644.42	770.85	133.39
Radius of Gyration (m)	0.89 ± 3.16	1.13 ± 4.06	0.91 ± 3.50	0.94 ± 2.47
LSI (no units)	579.48	410.67	696.49	352.31
IJI (%)	65.11	77.77	24.91	57.80
Total Edge (km)	6827.33	5025.35	10134.35	2238.16
Edge Density (m ha ⁻¹)	903.42	664.98	1423.19	314.31
PARA (m ⁻¹)	3.26 ± 0.92	3.07 ± 1.04	3.30 ± 0.91	3.13 ± 1.03

Forecasting and Evaluating Change

Our geospatial subtraction analysis yielded a clear visual depiction of relative community change across our target marshes (Figure 4). A shift refers to any change no matter how small in the following description. We found that, not only was there a vast reduction in *S. patens* in favor of *S. alterniflora* for the southern marsh as detailed previously, but there were also shifts in community structure across both marshes. For example, there were many small shifts in the northern marsh from *S. patens* to *S. alterniflora*, but also from *S. alterniflora* to *S. patens*. However, these were less intense than the changes from *S. patens* to *S. alterniflora* exhibited by the southern marsh. The southern marsh also exhibited some change from *S. alterniflora* to *S. patens* restricted to the banks of streams. All other shifts that involved water as a third class can be found in Figure S5. Our time series analysis elucidated distinct trends for *S. patens* in both marshes (Figure 5). The northern marsh saw losses of *S. patens* from 1213.90 ha in 2008 to 716.07 ha in 2010 and from 865.32 ha in 2013 to 638.99 ha in 2015. However, from 2006 to 2008 and 2010 to 2013, the northern marsh saw modest gains of *S. patens* and, from 2015 to 2019, saw gains leading to a cover of 937.87 ha that surpassed the original classified area of *S. patens* from 2006. Our forecasting of the northern marsh also modeled moderate gain over the next 5 years until 2024, where *S. patens* was predicted at the highest coverage since maximum *S. patens* in 2008 at 1158.16 ha. The southern marsh experienced stagnation or loss of *S. patens* over every span of years plotted in its time series, except for gains from 481.07 ha to 765.29 ha between 2010 and 2013. Forecasting predicted *S. patens* cover of 151.78 ha in 2022 and final *S. patens* cover of 84.70 ha in 2024.

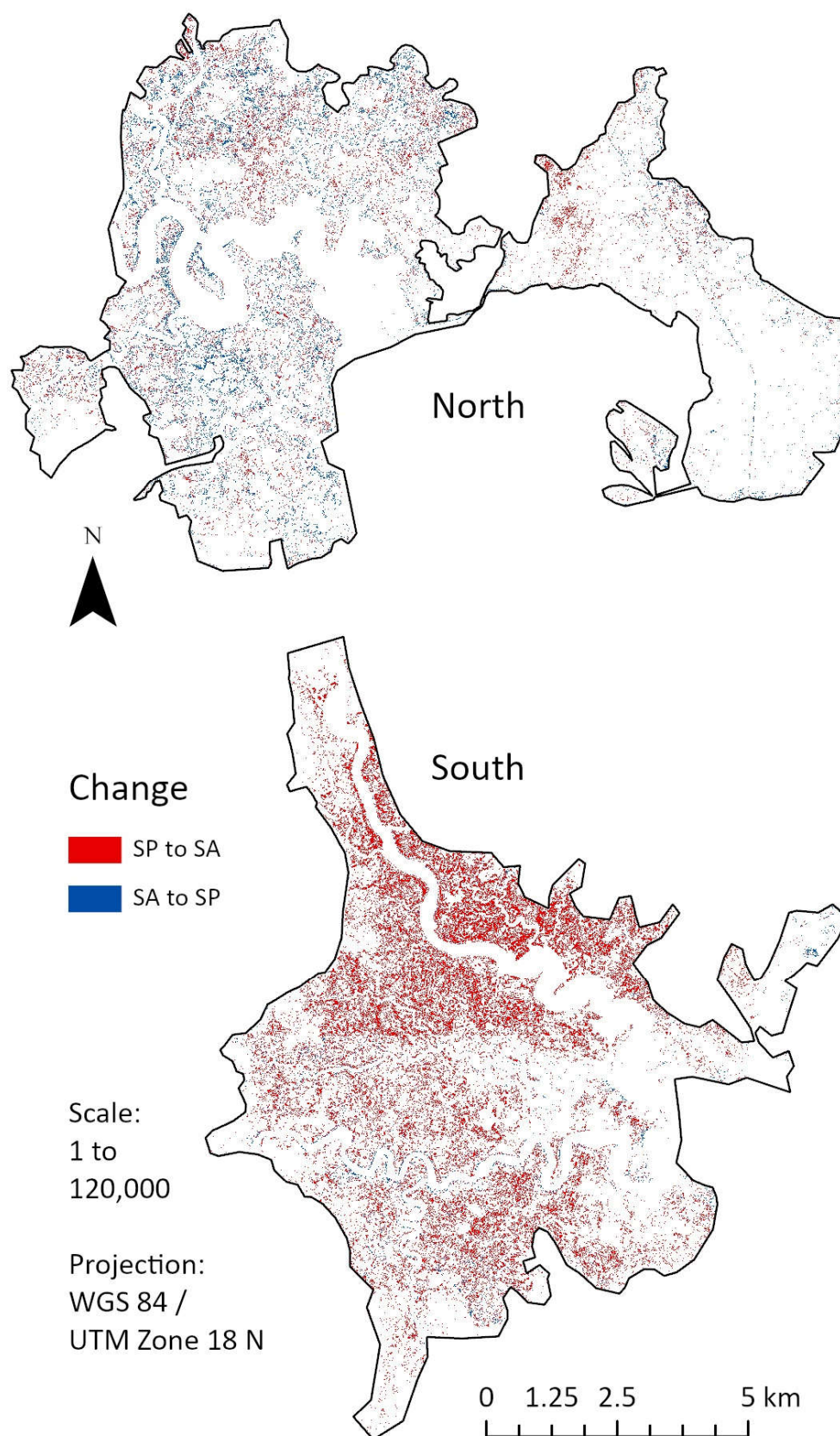


Figure 4. Geospatial community change from 2006 to 2019 for our target marshes. Note that majority of change occurs in the southern marsh from *S. patens* (SP) to *S. alterniflora* (SA). Northern marsh relative centroid is at 39° 33' 20" N, 74° 26' 26" W; southern marsh relative centroid is at 39° 18' 22" N, 74° 41' 42" W. Created in ArcGIS Pro, version 2.9.1 (Esri Inc. 2021).

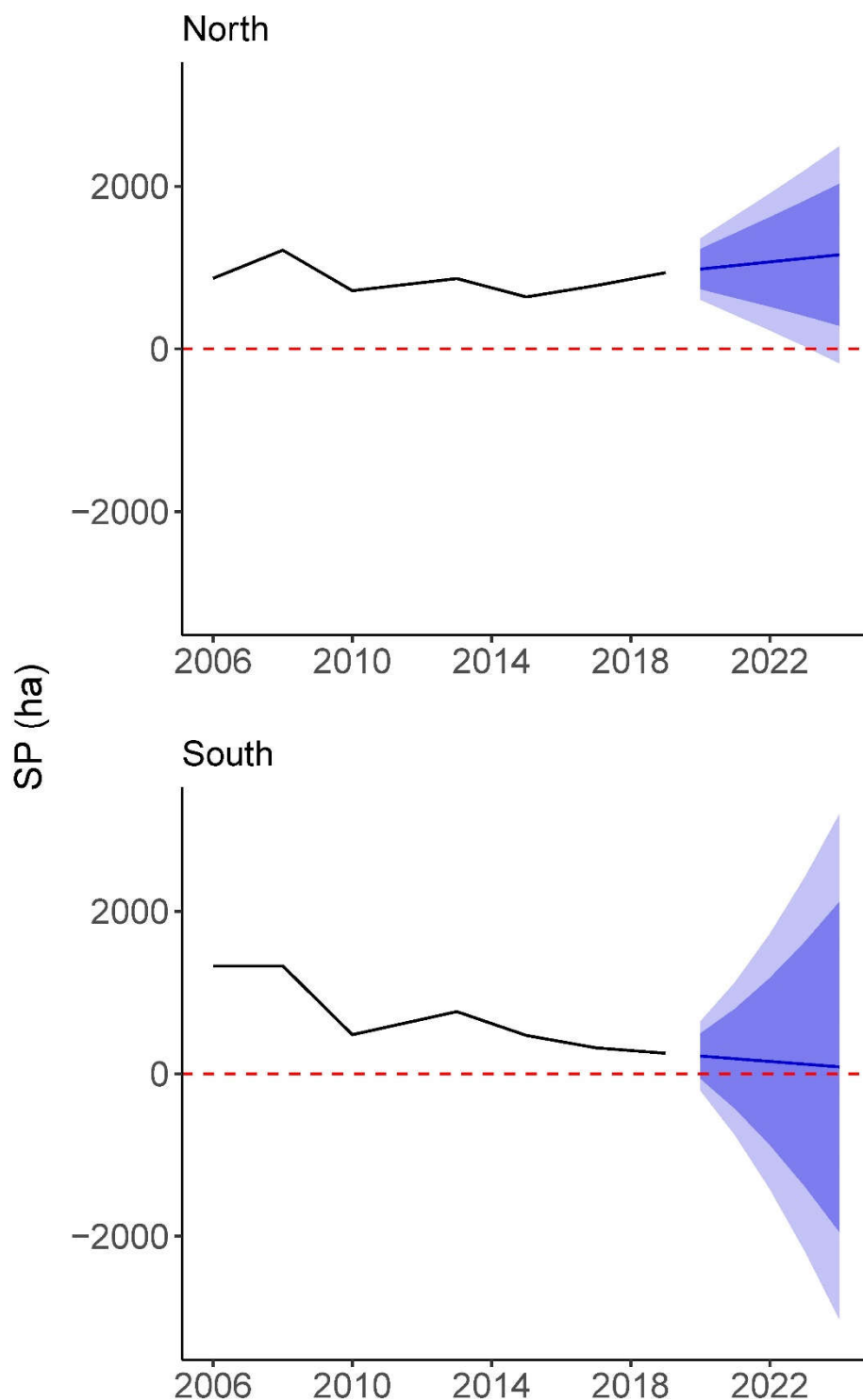


Figure 5. Time series depicting *S. patens* (SP) changes for our target marshes using imagery from 7 years between, and including, 2006 and 2019. Forecasting predicts future trends for *S. patens* with Holt's Linear Trend Confidence Interval where darker shaded regions are 80% confidence intervals and lighter regions are 95% confidence intervals. Created in R, version 4.1.3 (R Core Team 2022).

We found that models including streamflow and total N, but without their interaction, best predicted responses of *S. patens* for both the raw and interpolated data. Full model selection results can be found in Table S2. Though both streamflow ($\hat{\beta} = -1.40$, 95% credible interval = -2.06 to -0.71) and total N ($\hat{\beta} = -5.22$, 95% credible interval = -6.99 to -3.31) were strong predictors of *S. patens* loss, total N was the strongest predictor overall

for the interpolated data (the intercept overlapped no Bayesian credible intervals for streamflow and total N; Figure 6). For the raw data, streamflow was a strong predictor of *S. patens* loss ($\beta = -1.91$, 95% credible interval = -3.05 to -0.49), while total N was less likely to have an effect ($\beta = -1.73$, 95% credible interval = -5.53 to 2.48; intercept overlapped 80% Bayesian credible interval). In general, credible intervals for parameter estimates from the interpolated data were more compact, and thus more reliable, than those from the raw data.

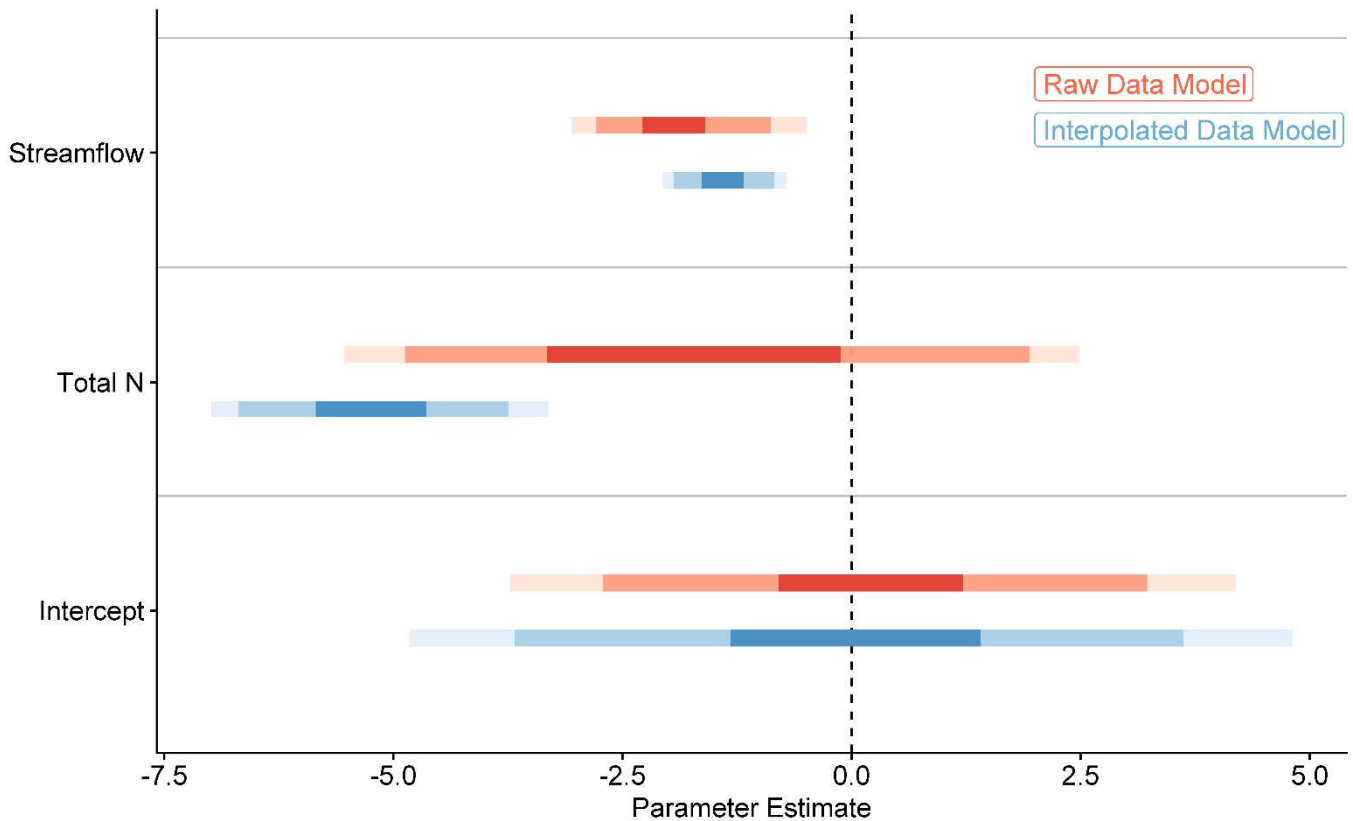


Figure 6. Parameter estimates for our best models following model selection in Table S2. The interpolated models included estimates for *S. patens* for years without available imagery. These were then compared to available streamflow and nutrient data from Lester et al. (2020). The darkest regions for each parameter are 50% Bayesian credible intervals, the moderately dark regions are 80% Bayesian credible intervals, and the lightest regions are 95% Bayesian credible intervals (Hespanhol 2019). Any parameter overlap of the dashed intercept can be treated as though that parameter is less likely to have driven losses of *S. patens*. Meanwhile, greater parameter distances from the intercept are greater likelihoods that the loss of *S. patens* is driven by that parameter. All models converged for markov chains before achieving maximum iterations. Created in R, version 4.1.3 (R Core Team 2022).

4. Discussion

Our analyses revealed substantial changes to the distributions of two foundation species along the New Jersey coast. However, the changes experienced by our target marshes were markedly different. Most notably, we found that our southern site suffered an 81.17% (1,087 ha) loss of *S. patens*, while our northern site experienced stochastic change. We found that this drastic loss of *S. patens* in the southern marsh was likely due to increased streamflow and nitrogen inputs. The loss of over 1,000 ha of *S. patens* in the southern marsh over 13 years appears to be one of the largest *S. patens* losses ever recorded, though we did not detect full scale losses of the salt marshes in general.

Past surveys from the U.S. government found a 1% loss of total salt marsh area along the Atlantic coast from 1998-2004 (Stedman and Dahl 2008) and a 0.4% reduction in total area from 2004-2009 (Dahl 2011). Although these losses declined over time, Campbell and

Wang (2020) found that much of the Tuckahoe-Corbin City Fish and Wildlife Management Area (the southern marsh of our study) lost a significant amount of aboveground biomass ranging from 142 to 1,031 g m⁻². The areas that saw the highest reduction in biomass appear to correspond with the areas where we saw the largest transformations of *S. patens* to *S. alterniflora*, which reflects findings that *S. patens* typically has larger aboveground carbon stocks (Elsey-Quirk et al. 2011; Snedden et al. 2015), often with equivalent amounts of live and dead biomass (Rippel et al. 2020). Thus, our results confirm drastic transformations found by Campbell and Wang (2020) and elucidate that these changes are likely due to shifting assemblages of foundation species despite a relatively small loss of Atlantic coast salt marshes overall in the past 20 years (Dahl 2011; Stedman and Dahl 2008). Forecasting of our marsh classifications for all years predicted a continuous decline in *S. patens* in the southern marsh and a relative gain in the northern marsh. This further exemplifies the stark differences seen between two marshes only 25 miles apart from one another. Although the conversion of *S. patens* to *S. alterniflora* has been shown on smaller scales (Donnelly and Bertness 2001; Warren and Niering 1993; Watson et al. 2016; Zajac et al. 2017), only a few examples exist in the literature of geographically close ecosystems with distinct changes in foundation species under similar disturbance conditions. In one example, Carey et al. (2017) reported distinct differences in elevation gain between two nearby marshes over a 10-year period, where one marsh was not keeping up with sea level rise while the other was, although there were no significant changes in foundation species in either marsh. Our results provide an example that similar geography, spatial location, and protected management between ecosystems may not predict similar changes to salt marsh foundation species over time.

Why did our target marshes change so disparately over the past 15 years? Notably, from 2006-2016 the Great Egg Harbor River feeding the southern marsh had >4× the streamflow, 2× the total nitrogen, and nearly 2× the total phosphorus than the Mullica River feeding the northern marsh. The results of our mixed-effects models indicated that streamflow and total N were important drivers of *S. patens* loss regardless of marsh and year for the interpolated data. Streamflow remained an important driver for the raw data, while total N was less predictive. Both marshes were inundated with the highest streamflow from their respective rivers in 2010, which corresponds to the greatest losses seen in the southern marsh. Furthermore, the southern marsh appears to experience losses throughout with a concentration along the Great Egg Harbor River (Figure 3), while changes seen in the northern marsh appear to be more stochastic. Thus, it is plausible that higher nutrient concentrations and higher average streamflow had already stressed the southern marsh, leading to a threshold collapse that resulted in drastic losses of *S. patens* over a relatively short time, as has been seen in other ecosystems (e.g., Boada et al. 2017; Connell et al. 2017; Liu et al. 2020a). Perhaps most critically, the relationships we found for losses of *S. patens*, as a result of higher streamflow and total N, are compatible with current knowledge of ecological dynamics in salt marshes of the Eastern US (Bertness 1991; Elsey-Quirk et al. 2019; Gedan and Bertness 2010; Snedden et al. 2015; Watson et al. 2016; Zajac et al. 2017). Analyzing interpolated *S. patens* cover was important as *S. patens* loss is not a stagnant process and is better understood as a trend over time. Furthermore, we were able to relate streamflow and nutrient data for years between imagery dates which allowed us to capture yearly trends more holistically. Our results show that trends may not be appropriately captured when only considering certain imagery dates as losses could be the result of lags or simply be caused by higher inputs in between imagery years. Similarly, the lack of coverage of our raw data was a probable cause of wider Bayesian credible intervals, and thus less credible results, versus those from the interpolated data.

Our landscape metrics analysis revealed only moderate differences in community structure for the northern and southern marshes in 2006, followed by profound changes in subsequent years (Table 1). One may have expected to find indicators of *S. patens* loss, such as lower elevations, higher edge densities, perimeter-to-edge ratios, and isolation, as these are known to have negative impacts on *S. patens* and its dependent communities

(Bertness 1991; Rippel et al. 2020; Wimp and Murphy 2021). The northern and southern marshes are similar in size and in 2006 had a similar amount of *S. patens*, similar average patch sizes, similar perimeter-to-edge ratios, and similar physical parameters. Further, the northern marsh was more fragmented, as measured by IJI, than the southern marsh in 2006. These results demonstrate that there was little indication of a massive shift in *S. patens* abundance in the southern marsh, which could be expected from patches with high perimeter-to-edge ratios, small areas, or low elevations (Delaney et al. 2000; Hartig et al. 2002; Rippel et al. 2020; Watson et al. 2016). Previous research has indicated that loss of *S. patens* can have substantial impacts on animal and microbial communities, such as the threatened salt sparrow (Bayard and Elphick 2011), specialist herbivores (Denno 1977), generalist predators (Wimp et al. 2011, 2019; Wimp and Murphy 2021), detritivorous snails (Johnson and Williams 2017; Zajac et al. 2017), and many others. As habitat specialists, these organisms will also be impacted by the increased isolation and fragmentation of these patches (Benoit and Askins 2002; Denno and Roderick 1991; Wimp et al. 2011, 2019; Wimp and Murphy 2021). Furthermore, many fish (Harrison-Day et al. 2021) and bird species (Ladin et al. 2020) are endemic to Eastern US salt marshes and utilize many of the above resources. Thus, the impacts of *S. patens* dieback on animals and other organisms dependent on *S. patens* should be investigated in the southern marsh.

Our results show that with the use of 1-m VHR imagery, simple yet practical machine learning methods can finely capture community transformations across broad geospatial and temporal scales. We achieved *S. patens* accuracy of 94.59% for the 2006 imagery and 100% for 2019, the highest observed in any literature thus far. We acknowledge that an accuracy of 100% is rare and may cause skepticism. Thus, we rigorously examined our landscapes for 2019 and confirmed that classifications of *S. patens* aligned extensively with our knowledge of *S. patens* from aerial imagery and ground-level observations (Figures S2 and S3). We have also given evidence that this result is substantiated with increasing testing data (Figure 2). Additionally, we saw overall accuracy >90% for all classification years, reaching upwards of 98.75% for 2019. Marshes in New Jersey's Atlantic coastal plain are heavily dominated by *S. alterniflora* and *S. patens*, which exist in nearly entirely separate patches that are visually distinct (Kennish et al. 2014; Watson et al. 2016; Wimp and Murphy 2021). Given the high classification accuracy of our methods, the use of VHR imagery in GEE would also be helpful for ecosystems which share the distinguishing quality of *Spartina* spp. marshes and for studies which seek to achieve a broader level of classification, such as for analyzing relative abundance of distinct communities that share a geographic space. GEE should be considered a cost-effective gateway into the world of machine learning for geospatial analyses. Since GEE is a cloud-based resource, its use could also lead to the development of more refined methods without needing to rely on immense personal computing power or high internet speeds. This potentially solves a lingering issue in broad-scale geospatial analyses, where large, high-resolution landscapes typically require intense computational resources with client-side software such as Arc products, R, or Python (Mutanga and Kumar 2019). Utilizing different types of data, such as near-infrared (Liu et al. 2020b), or other classification methods (e.g., random forest, naive Bayesian) would further extend our methods to a broader range of ecosystems that differ more intensely based on alternative data.

5. Conclusion

Access to substantial datasets as used in this project is a luxury we have in landscape ecology that is unparalleled in most other fields. However, past research has shown that adequately representing fine-scale dynamics across large areas can be difficult. Our results indicate that broad landscapes can be classified simply and effectively with powerful server-side analyses. Large changes in community structure are typically slow processes; our findings indicate that, for certain ecosystems, this is not the case. We showed that two geographically close marshes had distinctly different losses of *S. patens* over a 13-year period, with one marsh suffering an 81.17% loss and the other seeing little overall change.

Our results detail the context-dependency of habitat loss at the landscape scale, where one landscape can be experiencing a threshold for ecosystem collapse while a similar and nearby landscape experiences stochasticity. Further, our analysis of potential drivers of this loss revealed that increases in streamflow and total riverine nitrogen concentrations were both associated with losses in *S. patens*. These broad-scale results confirm plot level studies of the dominance of *S. alterniflora* over *S. patens* in higher tides and with higher nitrogen concentrations, illustrating that we cannot simply apply models of best-case scenarios to all similar ecosystems in a given area.

Supplementary Materials:

Fig. S1 Model accuracy for increasing numbers of randomly partitioned training data used in machine learning supervision. Analyses were continued at least 5 steps past the selected # of training data to ensure that we satisfied the overfitting clause. $X = 1080$ was chosen as a graphical cutoff as it was the entry before overfitting for the year with the greatest numbers of training data to reach equilibrium. Created in R, version 4.1.3 (R Core Team 2022).

Fig. S2 2019 RGB image classification of a roughly 350 ha sample region (*Spartina* spp. marsh in Galloway and Bass River, NJ; 39°32'54" N, 74°25'44" W) for cases with increasing breadths of training data. Pane A was trained with 240 total entries from the surrounding area (Accuracy = 93.3%), Pane B with 480 (Accuracy = 97.5%), Pane C with 720 (Accuracy = 98.3%), and Pane D with 960 (Accuracy = 98.8%). Pane E is the 960 (most accurate) training entry case for comparison with Pane F, a true color image. SA is *S. alterniflora* and SP is *S. patens*. Projection: WGS 84 / UTM Zone 18N. Created in ArcGIS Pro, version 2.9.1 (Esri Inc.).

Fig. S3 Geospatial example comparison of NAIP imagery (TC for true color) and our supervised classifications (ML for machine learning) used to confirm machine learning accuracy measures. These depictions are roughly 1/100th the total area of our marshes. *S. alterniflora*: dark green and *S. patens*: light green. Note the consistently accurate predictions for *S. patens*, even capturing exact shapes of patches. Furthermore, note the increase in marsh ponding captured for 2019 as a proxy for fine-scale dynamics accurately represented in our final models. Relative centroid is at 39° 17' 12.8" N, 74° 40' 26.3" W. Created in Google Earth Engine (Gorelick et al. 2017).

Fig. S4 Relative cover of *S. alterniflora* (SA) and *S. patens* (SP) for our target marshes from 2006 to 2019. Percentage values do not sum to 100 as water is not included, an aesthetic chosen to emphasize the target relationship. Created in R, version 4.1.3 (R Core Team 2022).

Fig. S5 Geospatial community change (2006-2019) for our target marshes. Note that most obvious changes occur from *S. patens* (SP) to *S. alterniflora* (SA) in the southern marsh. Northern marsh relative centroid is at 39° 33' 20" N, 74° 26' 26" W; southern marsh relative centroid is at 39° 18' 22" N, 74° 41' 42" W. Created in ArcGIS Pro, version 2.9.1 (Esri Inc. 2021).

Table S1 Proximal stream gauge data for our target marshes (modified from Lester et al. 2020). These parameters are reflective of relative inputs to the marshes and as such are used in this study as a proxy. The rivers used for each marsh are 1st order streams and are sustained via the confluence of other smaller rivers. Thus, they also represent the most dominant inputs of streamflow and nutrients to their respective marshes. Note the much larger streamflow and nitrogen inputs to the southern marsh. Total N included all measured nitrogen-based inputs. Total P included all measured phosphorus-based inputs.

Table S2 Model comparison results for environmental predictors of the total area of *S. patens* patches in each marsh. Models were compared using leave-one-out cross-validation (Vehtari et al. 2017). ELPD stands for the expected log pointwise predictive density. The farther away a model is from 0 ELPD, the less relative predictive power it has. Thus, the bolded central model is the best model for both raw and interpolated (INTRP) data. All models converged for markov chains before achieving maximum iterations.

Author Contributions: Conceptualization, T.M.R.; methodology, C.D.M.-D., V.S.; formal analyses, C.D.M.-D., V.S.; data curation, C.D.M.-D.; writing - original draft preparation, T.M.R., C.D.M.-D., V.S.; writing - review and editing, T.M.R., C.D.M.-D., G.M.W., V.S. All authors have read and agreed to the published version of the manuscript.

Funding: T.M.R., C.D.M.-D., and V.S. were supported through graduate research fellowships at Georgetown University. V.S. was supported by the National Science Foundation Graduate Research Fellowship under grant number 1937959.

Data Availability Statement: The raw data, manipulated data and R scripts used in this study's analyses are openly available in FigShare at <https://doi.org/10.6084/m9.figshare.19666488>.

Acknowledgments: We would like to thank Kaitlyn E. Minsavage-Davis for contributions to the synthesis of our machine learning methodology.

Conflicts of Interest: The authors declare no conflict of interest.

References

- Adkins, Z. 2009. NAIP 2008 Absolute Ground Control: From the Ground up. US Department of Agriculture, Washington, DC. https://www.fsa.usda.gov/Internet/FSA_File/naip_2008_controppt_summary.pdf. Accessed 23 March 2022.
- Alber, M., E.M. Swenson, S.C. Adamowicz, and I.A. Mendelsohn. 2008. Salt marsh dieback: an overview of recent events in the US. *Estuarine, Coastal and Shelf Science* 80:1–11. doi:10.1016/j.ecss.2008.08.009
- Artigas, F.J. and J. Yang. 2006. Spectral discrimination of marsh vegetation types in the New Jersey Meadowlands, USA. *Wetlands* 26:271–277. doi:10.1672/0277-5212(2006)26[271:SDOMVT]2.0.CO;2
- Artigas, F.J. and I.C. Pechmann. 2010. Balloon imagery verification of remotely sensed *Phragmites australis* expansion in an urban estuary of New Jersey, USA. *Landscape and Urban Planning* 95:105–112. doi:10.1016/j.landurbplan.2009.12.007
- Barbier, E.B., S.D. Hacker, C. Kennedy, E.W. Koch, A.C. Stier, and B.R. Silliman. 2011. The value of estuarine and coastal ecosystem services. *Ecological Monographs* 81:169–193. doi:10.1890/10-1510.1
- Bayard, T.S. and C.S. Elphick. 2011. Planning for sea-level rise: Quantifying patterns of saltmarsh sparrow (*Ammodramus caudacutus*) nest flooding under current sea-level conditions. *The Auk* 128:393–403. doi:10.1525/auk.2011.10178
- Benoit, L.K. and R.A. Askins. 2002. Relationship between habitat area and the distribution of tidal marsh birds. *The Wilson Bulletin* 114:314–323.
- Bertness, M.D. 1991. Zonation of *Spartina patens* and *Spartina alterniflora* in New England salt marsh. *Ecology* 72:138–148. doi:10.2307/1938909
- Boada, J., R. Arthur, D. Alonso, J.F. Pagès, A. Pessarrodona, S. Oliva, G. Ceccherelli, L. Piazzi, J. Romero, and T. Alcoverro. 2017. Immanent conditions determine imminent collapses: nutrient regimes define the resilience of macroalgal communities. *Proceedings of the Royal Society B* 284:20162814. doi:10.1098/rspb.2016.2814
- Broussard, W.P., J.M. Visser, and R.P. Brooks. 2020. Quantifying vegetation and landscape metrics with hyperspatial unmanned aircraft system imagery in a coastal oligohaline marsh. *Estuaries and Coasts* 45:1058–1069. doi:10.1007/s12237-020-00828-8
- Bürkner, P.-C. 2021. Bayesian Item Response Modeling in R with brms and Stan. *Journal of Statistical Software* 100:1–54. doi:10.18637/jss.v100.i05
- Campbell, A.D. and Y. Wang. 2019. High spatial resolution remote sensing for salt marsh mapping and change analysis at fire island national seashore. *Remote Sensing* 11:1107. doi:10.3390/rs11091107
- Campbell, A.D. and Y. Wang. 2020. Salt marsh monitoring along the mid-Atlantic coast by Google Earth Engine enabled time series. *PloS One* 15:e0229605. doi:10.1371/journal.pone.0229605
- Carey, J.C., K.B. Raposa, C. Wigand, and R.S. Warren. 2017. Contrasting decadal-scale changes in elevation and vegetation in two long island sound salt marshes. *Estuaries and Coasts* 40:651–661. doi:10.1007/s12237-015-0059-8
- Cheng, Y.-C. and S.-Y. Chen. 2003. Image classification using color, texture and regions. *Image and Vision Computing* 21:759–776. doi:10.1016/S0262-8856(03)00069-6
- Chmura, G.L., S.C. Anisfeld, D.R. Cahoon, and J.C. Lynch. 2003. Global carbon sequestration in tidal, saline wetland soils. *Global Biogeochemical Cycles* 17:1111. doi:10.1029/2002GB001917
- Connell, S.D., M. Fernandes, O.W. Burnell, Z. Doubleday, K.J. Griffin, A.D. Irving, J.Y.S. Leung, S. Owen, B.D. Russell, and L.J. Falkenberg. 2017. Testing for thresholds of ecosystem collapse in seagrass meadows. *Conservation Biology* 31:1196–1201. doi:10.1111/cobi.12951
- Crosby, S.C., D.F. Sax, M.E. Palmer, H.S. Booth, L.A. Deegan, M.D. Bertness, and H.M. Leslie. 2016. Salt marsh persistence is threatened by predicted sea-level rise. *Estuarine, Coastal and Shelf Science* 181:93–99. doi:10.1016/j.ecss.2016.08.018
- Dahl, T.E. 2006. Remote sensing as a tool for monitoring wetland habitat change. US Fish and Wildlife Service, Branch of Habitat Assessment, Fish and Wildlife Resource Centre, Onalaska, WI. <https://www.fws.gov/wetlands/Documents/Remote-Sensing-as-a-Tool-for-Monitoring-Wetland-Habitat-Change.pdf>. Accessed 20 March 2022.
- Dahl, T.E. 2011. Status and trends of wetlands in the conterminous united states 2004 to 2009. U.S. Department of the Interior, U.S. Fish and Wildlife Service, Washington, DC. <https://www.fws.gov/wetlands/documents/status-and-trends-of-wetlands-in-the-conterminous-united-states-2004-to-2009.pdf>. Accessed 10 March 2022.
- Deegan, L.A., D.S. Johnson, R.S. Warren, B.J. Peterson, J.W. Fleeger, S. Fagherazzi, and W.M. Wollheim. 2012. Coastal eutrophication as a driver of salt marsh loss. *Nature* 490:388–392. doi:10.1038/nature11533
- Delaney, T.P., J.W. Webb, and T.J. Minello. 2000. Comparison of physical characteristics between created and natural estuarine marshes in Galveston Bay, Texas. *Wetlands Ecology and Management* 8:343–352. doi:10.1023/A:1008439420830

- Denno, R.F. 1977. Comparison of the assemblages of sap-feeding insects (Homoptera-Hemiptera) inhabiting two structurally different salt marsh grasses in the genus *Spartina*. *Environmental Entomology* 6:359–372. doi:10.1093/ee/6.3.359
- Denno, R.F. and G.K. Roderick. 1991. Influence of patch size, vegetation texture, and host plant architecture on the diversity, abundance, and life history styles of sapfeeding herbivores. In *Habitat Structure*, eds. S.S. Bell, E.D. McCoy, and H.R. Mushinsky, 169–196. Dordrecht:Springer.
- Donnelly, J.P. and M.D. Bertness. 2001. Rapid shoreward encroachment of salt marsh cordgrass in response to accelerated sea-level rise. *Proceedings of the National Academy of Sciences* 98:14218–14223. doi:10.1073/pnas.251209298
- Ellison, A.M. 2019. Foundation species, non-trophic interactions, and the value of being common. *iScience* 13:254–268. doi:10.1016/j.isci.2019.02.020
- Else-Quirk, T., D.M. Seliskar, C.K. Sommerfield, and J.L. Gallagher. 2011. Salt marsh carbon pool distribution in a mid-Atlantic lagoon, USA: sea level rise implications. *Wetlands* 31:87–99. doi:10.1007/s13157-010-0139-2
- Else-Quirk, T., S.A. Graham, I.A. Mendelssohn, G. Snedden, J.W. Day, R.R. Twilley, G. Shaffer, L.A. Sharp, J. Pahl, and R.R. Lane. 2019. Mississippi river sediment diversions and coastal wetland sustainability: Synthesis of responses to freshwater, sediment, and nutrient inputs. *Estuarine, Coastal and Shelf Science* 221:170-183. doi:10.1016/j.ecss.2019.03.002
- Earth Resources Observation and Science (EROS) Center. 2018. USGS EROS Archive - Aerial Photography - National Agriculture Imagery Program (NAIP). <https://www.usgs.gov/centers/eros/science/usgs-eros-archive-aerial-photography-national-agriculture-imagery-program-naip>. Accessed 10 February 2022.
- Esri Inc. 2021. ArcGIS Pro (Version 2.9.1). <https://www.esri.com/en-us/arcgis/products/arcgis-pro/overview>
- FitzGerald, D.M. and Z. Hughes. 2019. Marsh processes and their response to climate change and sea-level rise. *Annual Review of Earth and Planetary Sciences* 47:481–517. doi:10.1146/annurev-earth-082517-010255
- Gedan, K.B., B.R. Silliman, and M.D. Bertness. 2009. Centuries of human-driven change in salt marsh ecosystems. *Annual Reviews of Marine Science* 1:117-141. doi:10.1146/annurev.marine.010908.163930
- Gedan, K.B. and M.D. Bertness. 2010. How will warming affect the salt marsh foundation species *Spartina patens* and its ecological role? *Oecologia* 164:479–487. doi:10.1007/s00442-010-1661-x
- Gedan, K.B., M.L. Kirwan, E. Wolanski, E.B. Barbier, and B.R. Silliman. 2011. The present and future role of coastal wetland vegetation in protecting shorelines: Answering recent challenges to the paradigm. *Climatic Change* 106:7–29. doi:10.1007/s10584-010-0003-7
- Gholamy, A., V. Kreinovich, and O. Kosheleva. 2018. Why 70/30 or 80/20 relation between training and testing sets: A pedagogical explanation. Departmental Technical Reports (CS), University of Texas at El Paso, El Paso, TX. https://scholarworks.utep.edu/cs_techrep/1209/. Accessed 20 February 2022.
- Gilmore, M.S., E.H. Wilson, N. Barrett, D.L. Civco, S. Prisloe, J.D. Hurd, and C. Chadwick. 2008. Integrating multi-temporal spectral and structural information to map wetland vegetation in a lower Connecticut River tidal marsh. *Remote Sensing of Environment* 112:4048–4060. doi:10.1016/j.rse.2008.05.020
- Gorelick, N., M. Hancher, M. Dixon, S. Ilyushchenko, D. Thau, and R. Moore. 2017. Google Earth Engine: Planetary-scale geospatial analysis for everyone. *Remote Sensing of Environment* 202:18–27. doi:10.1016/j.rse.2017.06.031
- Green, K.C. and J.S. Armstrong. 2015. Simple versus complex forecasting: the evidence. *Journal of Business Research* 68:1678–1685. doi:10.1016/j.jbusres.2015.03.026
- Hardisky, M.A., M.F. Gross, and V. Klemas. 1986. Remote sensing of coastal wetlands. *Bioscience* 36:453–460. doi:10.2307/1310341
- Harrison-Day, V., V. Prahalad, J.B. Kirkpatrick, and M. McHenry. 2021. A systematic review of methods used to study fish in saltmarsh flats. *Marine and Freshwater Science* 72:149-162. doi:10.1071/MF20069
- Hartig, E.K., V. Gornitz, A. Kolker, F. Mushacke, and D. Fallon. 2002. Anthropogenic and climate-change impacts on salt marshes of Jamaica Bay, New York City. *Wetlands* 22:71–89. doi:10.1672/0277-5212(2002)022[0071:AACCIO]2.0.CO;2
- Hespanhol, L., C.S. Vallio, L.M. Costa, and B.T. Saragiotto. 2019. Understanding and interpreting confidence and credible intervals around effect estimates. *Brazilian Journal of Physical Therapy* 23:290-301. doi:10.1016/j.bjpt.2018.12.006
- Hyndman, R.J. and Y. Khandakar. 2008. Automatic time series forecasting: the forecast package for R. *Journal of Statistical Software* 27:1–22. doi:10.18637/jss.v027.i03
- Jiang, J., F. Liu, Y. Xu, and H. Huang. 2019. Multi-spectral RGB-NIR image classification using double-channel CNN. *IEEE Access* 7:20607–20613. doi:10.1109/ACCESS.2019.2896128
- Johnson, D.S. and B.L. Williams. 2017. Sea level rise may increase extinction risk of a saltmarsh ontogenetic habitat specialist. *Ecology and Evolution* 7:7786–7795. doi:10.1002/ece3.3291
- Kennish, M.J., M.S. Meixler, G. Petruzzelli, and B. Fertig. 2014. Tuckerton Peninsula salt marsh system: a sentinel site for assessing climate change effects. *Bulletin of the New Jersey Academy of Science* 59:1–5. doi:10.7282/T3348NBS
- Kirwan, M.L. and S.M. Mudd. 2012. Response of salt-marsh carbon accumulation to climate change. *Nature* 489:550–553. doi:10.1038/nature11440
- Kirwan, M.L., J.A. Langley, G.R. Guntenspergen, and J.P. Megonigal. 2013. The impact of sea-level rise on organic matter decay rates in Chesapeake Bay brackish tidal marshes. *Biogeosciences* 10:1869–1876. doi:10.5194/bg-10-1869-2013
- Kopp, R.E., C. Andrews, A. Broccoli, A. Garner, D. Kreeger, R. Leichenko, N. Lin, C. Little, J.A. Miller, J.K. Miller, K.G. Miller, R. Moss, P. Orton, A. Parris, D. Robinson, W. Sweet, J. Walker, C.P. Weaver, K. White, M. Campo, M. Kaplan, J. Herb, and L. Auermuller. 2019. New jersey's rising seas and changing coastal storms: report of the 2019 science and technical advisory panel. Rutgers, The State University of New Jersey. Prepared for the New Jersey Department of Environmental Protection, Trenton,

- New Jersey. <https://www.nj.gov/dep/climatechange/pdf/nj-rising-seas-changing-coastal-storms-stap-report.pdf>. Accessed 17 April 2022.
- Krause, J.R., E.B. Watson, C. Wigand, and N. Maher. 2019. Are tidal salt marshes exposed to nutrient pollution more vulnerable to sea level rise? *Wetlands* 40:1–10. doi:10.1007/s13157-019-01254-8
- Krzywinski, M. and N. Altman. 2017. Classification and regression trees. *Nature Methods* 14:757–758. doi:10.1038/nmeth.4370
- Ladin, Z.S., W.A. Wiest, M.D. Correll, E.L. Tymkiw, M. Conway, B.J. Olsen, C.S. Elphick, W.L. Thompson, and W.G. Shriver. 2020. Detection of local-scale population declines through optimized tidal marsh bird monitoring design. *Global Ecology and Conservation* 23:e01128. doi:10.1016/j.gecco.2020.e01128
- Langley, J.A. and J.P. Megonigal. 2010. Ecosystem response to elevated CO₂ levels limited by nitrogen-induced plant species shift. *Nature* 466:96–99. doi:10.1038/nature09176
- Lester, L.A., C. Kunz, L. Lager, and N.A. Procopio. 2020. Water quality trends in nutrients in new jersey streams, water years 1971–2016. New Jersey Department of Environmental Protection, Division of Science and Research, Trenton, NJ. <https://www.nj.gov/dep/dsr/wq/water-quality-trends-nutrients-1971-2016.pdf>. Accessed 07 June 2022.
- Liu, Y., L. He, S. Hilt, R. Wang, H. Zhang, and G. Ge. 2020a. Shallow lakes at risk: nutrient enrichment enhances top-down control of macrophytes by invasive herbivorous snails. *Freshwater Biology* 66:436–446. doi:10.1111/fwb.13649
- Liu, X., H. Liu, P. Datta, J. Frey, and B. Koch. 2020b. Mapping an invasive plant *Spartina alterniflora* by combining an ensemble one-class classification algorithm with a phenological NDVI time-series analysis approach in middle coast of Jiangsu, China. *Remote Sensing* 12:4010. doi:10.3390/rs12244010
- Mcowen, C.J., L.V. Weatherdon, J.-W.V. Bochove, E. Sullivan, S. Blyth, C. Zockler, D. Stanwell-Smith, N. Kingston, C.S. Martin, M. Spalding, and S. Fletcher. 2017. A global map of saltmarshes. *Biodiversity Data Journal* 5:e11764. doi:10.3897/BDJ.5.e11764
- Mueller, P., T.J. Mozdzer, J.A. Langley, L.R. Aoki, G.L. Noyce, and J.P. Megonigal. 2020. Plant species determine tidal wetland methane response to sea level rise. *Nature Communications* 11:5154. doi:10.1038/s41467-020-18763-4
- Mutanga, O. and L. Kumar. 2019. Google earth engine applications. *Remote Sensing* 11:591. doi:10.3390/rs11050591
- Raghukumar, S. 2017. *Fungi in coastal and oceanic marine ecosystems: marine fungi*. Cham:Springer.
- R Core Team. 2022. R: a language and environment for statistical computing. R Foundation for Statistical Computing, Vienna, Austria. <https://www.R-project.org/>.
- Rippel, T.M., E.Q. Mooring, J. Tomasula, and G.M. Wimp. 2020. Habitat edge effects decrease litter accumulation and increase litter decomposition in coastal salt marshes. *Landscape Ecology* 35:2179–2190. doi:10.1007/s10980-020-01108-3
- Schepers, L., M. Kirwan, G. Guntenspergen, and S. Temmerman. 2016. Spatio-temporal development of vegetation die-off in a submerging coastal marsh. *Limnology and Oceanography* 62:137–150. doi:10.1002/lno.10381
- Simas, T., J.P. Nunes, and J.G. Ferreira. 2001. Effects of global climate change on coastal salt marshes. *Ecological Modelling* 139:1–15. doi:10.1016/S0304-3800(01)00226-5
- Snedden, G.A., K. Cretini, and B. Patton. 2015. Inundation and salinity impacts to above- and belowground productivity in *Spartina patens* and *Spartina alterniflora* in the Mississippi River deltaic plain: implications for using river diversions as restoration tools. *Ecological Engineering* 81:133–139. doi:10.1016/j.ecoleng.2015.04.035
- Stedman, S.-M. and T.E. Dahl. 2008. Status and trends of wetlands in the coastal watersheds of the eastern United States 1998 to 2004. National Oceanic and Atmospheric Administration, National Marine Fisheries Service and U.S. Department of the Interior, Fish and Wildlife Service, Washington, DC. <https://www.fws.gov/wetlands/documents/Status-and-Trends-of-Wetlands-in-the-Coastal-Watersheds-of-the-Eastern-United-States-1998-to-2004.pdf>. Accessed 15 March 2022.
- Stolar, M.N., M. Lech, R.S. Bolia, and M. Skinner. 2017. Real time speech emotion recognition using RGB image classification and transfer learning. 2017 11th International Conference on Signal Processing and Communication Systems (ICSPCS) 1–8. doi:10.1109/ICSPCS.2017.8270472
- Suir, G.M., C.E. Sasser, and J.M. Harris. 2020. Use of remote sensing and field data to quantify the performance and resilience of restored Louisiana wetlands. *Wetlands* 40:2643–2658. doi:10.1007/s13157-020-01344-y
- Vehtari, A., A. Gelman, and J. Gabry. 2017. Practical Bayesian model evaluation using leave-one-out cross-validation and WAIC. *Statistics and Computing* 27:1413–1432. doi:10.1007/s11222-016-9696-4
- Warren, R.S. and W.A. Niering. 1993. Vegetation change on a northeast tidal marsh: interaction of sea-level rise and marsh accretion. *Ecology* 74:96–103. doi:10.2307/1939504
- Watson, E.B., K. Szura, C. Wigand, K.B. Raposa, K. Blount, and M. Cencer. 2016. Sea level rise, drought and the decline of *Spartina patens* in New England marshes. *Biological Conservation* 196:173–181. doi:10.1016/j.biocon.2016.02.011
- Watson, E.B., C. Wigand, E.W. Davey, H.M. Andrews, J. Bishop, and K.B. Raposa. 2017. Wetland loss patterns and inundation-productivity relationships prognosticate widespread salt marsh loss for southern New England. *Estuaries and Coasts* 40:662–681. doi:10.1007/s12237-016-0069-1
- Weis, J.S., E.B. Watson, B. Ravit, C. Harman, and M. Yepsen. 2021. The status and future of tidal marshes in New Jersey faced with sea level rise. *Anthropocene Coasts* 4:168–192. doi:10.1139/anc-2020-0020
- Wigand, C., E.B. Watson, R. Martin, D.S. Johnson, R.S. Warren, A. Hanson, E. Davey, R. Johnson, and L. Deegan. 2018. Discontinuities in soil strength contribute to destabilization of nutrient-enriched creeks. *Ecosphere* 9:e02329. doi:10.1002/ecs2.2329
- Wimp, G.M. and S.M. Murphy. 2021. Habitat edges alter arthropod community composition. *Landscape Ecology* 36:2849–2861. doi:10.1007/s10980-021-01288-6
- Wimp, G.M., S.M. Murphy, D. Lewis, and L. Ries. 2011. Do edge responses cascade up or down a multi-trophic food web? *Ecology Letters* 14:863–870. doi:10.1111/j.1461-0248.2011.01656.x

- Wimp, G.M., L. Ries, D. Lewis, and S.M. Murphy. 2019. Habitat edge responses of generalist predators are predicted by prey and structural resources. *Ecology* 100:e02662. doi:10.1002/ecy.2662
- Ying, X. 2019. An overview of overfitting and its solutions. *Journal of Physics: Conference Series* 1168:022022. doi:10.1088/1742-6596/1168/2/022022
- Zajac, R., E. Kelly, D. Perry, and I. Espinosa. 2017. Population ecology of the snail *Melampus bidentatus* in changing salt marsh landscapes. *Marine Ecology* 38:e12420. doi:10.1111/maec.12420